



**HAL**  
open science

# Optimal Control by Transmit Frequency in Tissue Harmonic Imaging

Sébastien Ménigot, Jean-Marc Girault

► **To cite this version:**

Sébastien Ménigot, Jean-Marc Girault. Optimal Control by Transmit Frequency in Tissue Harmonic Imaging. Acoustics 2012, Apr 2012, Nantes, France. pp.2863-2868. hal-00703029

**HAL Id: hal-00703029**

**<https://hal.science/hal-00703029>**

Submitted on 31 May 2012

**HAL** is a multi-disciplinary open access archive for the deposit and dissemination of scientific research documents, whether they are published or not. The documents may come from teaching and research institutions in France or abroad, or from public or private research centers.

L'archive ouverte pluridisciplinaire **HAL**, est destinée au dépôt et à la diffusion de documents scientifiques de niveau recherche, publiés ou non, émanant des établissements d'enseignement et de recherche français ou étrangers, des laboratoires publics ou privés.

# Optimal Control by Transmit Frequency in Tissue Harmonic Imaging

Sébastien Ménigot and Jean-Marc Girault

April 26, 2012

Ultrasound imaging systems usually work in open loop. The system control is thus a sine wave whose frequency is often fixed around two-thirds of the center frequency of the transducer in tissue harmonic imaging. However, this choice requires a knowledge of the transducer and does not take into account the medium properties. Our aim is to seek the command which maximizes the tissue harmonic contrast. We proposed an iterative optimization algorithm that automatically sought for the optimal frequency of the command. Both experimentally and in simulation, its value did not correspond to the usual value. The contrast can be improved by 5 dB. By providing a closed loop system, the system automatically proposes the optimal control without any a priori knowledge of the system or of the medium explored.

## 1 Introduction

Over the past twenty years, improvements in sensitivity of medical ultrasound imaging systems have provided more accurate medical diagnoses. Microbubble contrast agents has been introduced in the early 90's. Initially, the linear interactions between the microbubbles and the ultrasound waves were only operated in B-mode, to increase the contrast between the tissue and the microbubbles. However, the use of ultrasound contrast imaging was revolutionized in clinical practice when the nonlinear interaction was taken into account [1]. This revolution was so important that the tissue imaging used this principle [2] and actual commercial ultrasound scanner propose the tissue harmonic imaging by default.

However, obtaining an ideal method has been limited by a good separation of the harmonic components. This good separation requires a limited pulse bandwidth, which reduces the axial resolution as in second harmonic imaging [3]. Several imaging methods have been proposed to improve contrast and/or resolution. Some best-known techniques have been only based on post-processings, such as second harmonic imaging [3], third harmonic imaging [4]. Some techniques have been based on post-processings with discrete or continuous encoding. This encoding can be applied to the amplitude, phase or frequency of the ultrasound wave transmitted, such as pulse inversion [5, 6], power modulation [7, 3] and chirp imaging [8, 9].

For optimally using these methods, the setting parameters must be correctly adjusted. Unfortunately, up to now, no optimization process, which can provides the best contrast, the best resolution or the best compromise between contrast and resolution, exists. Indeed, the problem solution often requires inaccessible knowledges *a priori* of the medium and the transducer. Consequently, the transmit frequency was only set to the two-thirds of the transducer centre frequency [10] from empirical inference.

In this study, we propose to solve the transmit frequency choice through the concept of the optimal command [11]. We replaced thus the existing system by a closed loop system whose the transmit frequency was selected by feedback [12]. The optimization implementation required to specify the cost-function. The latter must be chosen by taking into account

the user's needs and the medical application. Here, in tissue harmonic imaging, the cost-function was the contrast harmonic to fundamental ratio (*CHFR*) in order to maximize the harmonic components and simultaneously minimize the fundamental component. Moreover, to complete our approach, the harmonic response detection was ensuring by the second harmonic imaging [3], since it is one of the most commonly used methods.

Finally, the optimization problem can be written from a formal point of view as follows:

$$f^* = \arg \max_f (CHFR(f)), \quad (1)$$

where  $f^*$  is the optimal transmit frequency which provides the best *CHFR*. We propose an iterative approach to find the optimal transmit frequency  $f^*$ .

## 2 Closed-loop Imaging System

The principle of tissue harmoning imaging including feedback is described in Fig. 1. At the iteration  $k$ , a pulse  $x_k(t)$  with a frequency  $f_k$  was transmitted. Its echo  $y_k(t)$  was filtered around  $2f_k$  to form a radiofrequency line of the harmonic image  $I_k$ . From the *CHFR* measured on this image  $I_k$ , a new transmit frequency  $f_{k+1}$  was computed by the algorithm to optimize the *CHFR* on the next image  $I_{k+1}$ .

### 2.1 Transmitted Signal

The pulse signal  $x_k(t)$  at transmit frequency  $f_k$  was computed digitally with Matlab (Mathworks, Natick, MA, USA):

$$x_k(t) = A \cdot w_k(t). \quad (2)$$

The sinus modulated by a Gaussian function [3]  $w_{k,p}(t)$  was constructed such as:

$$w_k(t) = \exp\left[-\frac{(t-t_0)^2}{\frac{N_c}{2f_k}}\right] \sin(2\pi f_k t), \quad (3)$$

where  $t$  is the time,  $t_0$  the time for which the Gaussian function is maximum,  $N_c$  the cycle number. Note that to limit

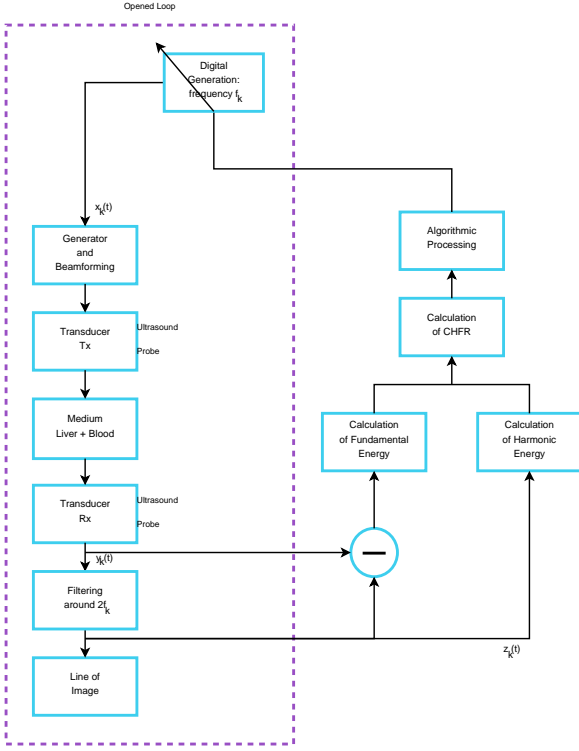


Figure 1: Block diagram of adaptive tissue harmonic imaging.

direct transmission around harmonic frequencies, the transducer bandwidth must be shared between the transmit and receive bandwidths [3]. The cycle number  $N_c$  was set so that the transmit bandwidth was equal to the half-bandwidth of the transducer.

The amplitude of the driving pressure  $A$  was then adjusted so that the power of the pulse  $x_k(t)$  was constant:

$$A = \sqrt{\frac{A_0^2 \cdot P_{x_{ref}}}{P_w}}, \quad (4)$$

where  $A_0$  is the driving pressure amplitude of the reference signal  $x_{ref}$ . This signal  $x_{ref}$  was calculated at the transducer centre frequency. Its power  $P_{x_{ref}}$  constituted the reference power, while  $P_w$  was the power of the signal  $w_k$ . The power of the transmitted wave thus remained constant by adjusting the amplitude signal  $A$ .

## 2.2 Cost-function

In the receiver, the  $CHFR_k$  was computed as the ratio of the harmonic power  $P_{h,k}$  backscattered and the fundamental power  $P_{f,k}$ :

$$CHFR_k = 10 \cdot \log_{10} \left( \frac{P_{h,k}}{P_{f,k}} \right), \quad (5)$$

The harmonic power was measured from the filtered echo  $z_k(t)$  and the fundamental power was measured from the fundamental echo which was equals to the difference between  $y_k(t)$  and  $z_k(t)$ . The harmonic echo  $z_k(t)$  formed the harmonic image by filtering  $y_k(t)$  at  $2f_k$  and with a bandwidth equal to the half-bandwidth of the transducer.

The gain  $G_{dB}$  was also defined between the optimized system and the non-optimized system. The  $CHFR$  obtained

with the non-optimized system was determined at the two-thirds of the transducer centre frequency  $2/3f_c$  [10]. The contrast gain  $G_{dB}$  is obtained by the next equation:

$$G_{dB} = \frac{CHFR(f^*)}{CHFR(2/3f_c)}. \quad (6)$$

## 2.3 Iterative Optimization Algorithm

The algorithm was based on the principle of the gradient descent [13]. It determined a new transmit frequency  $f_{k+1}$  for the next pulse to optimize the  $CHFR_{k+1}$  by the following recurrence relation:

$$f_{k+1} = f_k + \mu_k \cdot d_k, \quad (7)$$

The first coefficient  $\mu_k$  set the speed convergence such as:

$$\mu_k = \begin{cases} 0 & \text{if } k \leq 3; \\ \Delta f & \text{if } k = 4; \\ \mu_{k-1} & \text{if } \text{sgn}(\nabla CHFR(f_k)) = \text{sgn}(\nabla CHFR(f_{k-1})); \\ \frac{\mu_{k-1}}{2} & \text{if } \text{sgn}(\nabla CHFR(f_k)) \neq \text{sgn}(\nabla CHFR(f_{k-1})). \end{cases} \quad (8)$$

where  $\Delta f$  fixed at 100 kHz provided the best compromise between convergence speed and robustness,  $\text{sgn}(t)$  the sign function that is equal to 1 if  $t > 0$ , 0 if  $t = 0$  and  $-1$  if  $t < 0$ , and the  $CHFR$  gradient defined by:

$$\nabla CHFR(f_k) = \frac{CHFR_k - CHFR_{k-1}}{f_k - f_{k-1}}. \quad (9)$$

The second coefficient  $d_k$  set the direction such as:

$$d_k = \begin{cases} 1 & \text{if } k \leq 3; \\ 1 & \text{if } \text{sgn}(\nabla CHFR(f_k)) = \text{sgn}(\nabla CHFR(f_{k-1})); \\ -1 & \text{if } \text{sgn}(\nabla CHFR(f_k)) \neq \text{sgn}(\nabla CHFR(f_{k-1})). \end{cases} \quad (10)$$

In order to compute  $\mu_k$  and  $d_k$ , the system operated in open-loop for the first three iterations ( $k = \{1, 2, 3\}$ ). The first three frequencies  $f_1$ ,  $f_2$  and  $f_3$  were chosen initially. Their good choice could increase the convergence speed, but it was not decisive to reach the optimal  $CHFR$ , when the cost-function was concave.

## 3 Evaluation of the Method in Simulations

### 3.1 Simulation Model

The simulation model followed the same process as the experimental setup (Fig. 1).

A pulse signal was generated digitally at iteration  $k$  by the equation 2. Note that the pressure levels  $A_0$  was 400 kPa and the number cycle  $N_c$  was 4 to restrict the pulse bandwidth at the half-bandwidth of the transducer. However before sending this signal to the ultrasound probe, a beamforming step was added. The linear sweeping [14] enabled to focalized at 15 mm-depth with eight elements of the ultrasound probe. The pulse signal were then filtered by the transfer function of the ultrasound probe; centred at 3.5 MHz with a fractional bandwidth of 63% to  $-3$  dB.

This wave nonlinearly propagated in a liver-mimicking medium where the properties was described in table 1. In

Table 1: Mechanical Properties of the Medium Explored [14].

Liver	$\rho_1$	$N(1050 \text{ kg/m}^3, 30 \text{ kg}^2/\text{m}^6)$
	$c_1$	$N(1578 \text{ m/s}, 30 : \text{m}^2/\text{s}^2)$
Blood	$\rho_2$	$N(1060 \text{ kg/m}^3, 2.5 \text{ kg}^2/\text{m}^6)$
	$c_2$	$N(1584 : \text{m/s}, 2.5 : \text{m}^2/\text{s}^2)$

this medium, a 10 mm-diameter artery was at 15 mm of the surface. Moreover, the wave propagation was solved by the model developed by Anderson [15].

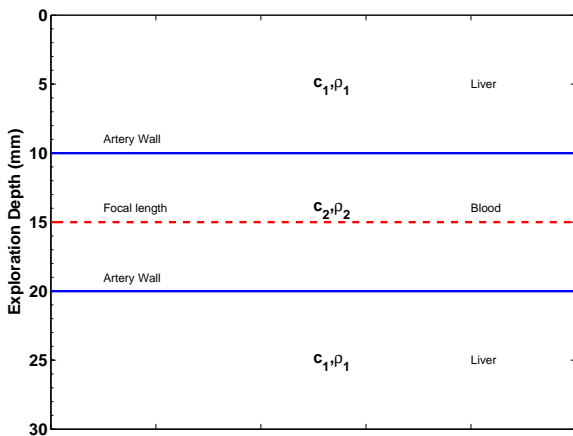


Figure 2: Grid of Medium Properties:  $c$  is the wave celerity and  $\rho$  is the density. The ultrasound probe was at the depth of 0 mm.

Finally, the echoes were measured and filtered by the transfer function of the same ultrasound probe to form a radiofrequency line.

### 3.2 Simulation Results

The empirical optimization was the first simulation presented in Fig. 3 by a dashed line. The results represent the  $CHFR$  as a function of the transmit frequency. The transmit frequency was swept by step of 0.125 MHz between 1 and 4 MHz. Firstly, the  $CHFR$  had a global maximum. This result showed that the  $CHFR$  can be improved by properly choosing the transmit frequency. This property was also interesting, because an automatic search could be achieved more easily by a gradient algorithm. Secondly, the maximum value of the  $CHFR$  was  $-29$  dB at 1.625 MHz and the gain  $G_{dB}$  was 8.3 dB. This result showed that the best transmit frequency was not the two-thirds of the transducer centre frequency. This point confirms again the necessity of optimizing the imaging process.

The maximum  $CHFR$  was then automatically sought using the gradient algorithm. The Fig. 3 shows the  $CHFR$  measured at each iteration  $k$  by a solid line. The transmit frequency converged to a stable value after height iterations at 1.6 MHz. Note that the  $CHFR$  and the gain  $G_{dB}$  obtained automatically were the same than those obtained empirically in the first simulation.

To sum up, the results in Fig. 3 confirm the necessity of optimizing the imaging system. It was possible to find

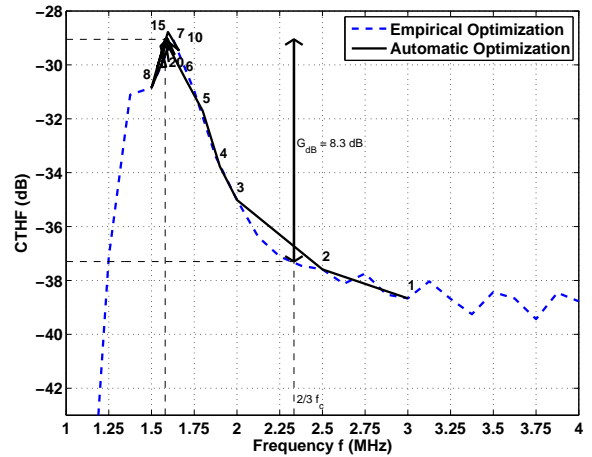


Figure 3: Simulation of the  $CHFR$  optimization. The dashed line represents an empirical optimization and the solid line represents an automatic optimization by iterative searching of the optimal transmit frequency.

automatically the transmit frequency which maximized the  $CHFR$ . No *a priori* knowledge was required, except for the choice of the first three transmit frequencies which impacted the speed of convergence.

As an illustration, the Fig. 4 represents the image for the two-thirds of the transducer centre frequency and the image for the optimal frequency  $f^*$  with logarithm compression. At the top of the images, the liver harmonic response was stronger with the optimal frequency. The contrast between the top (liver) and the middle (blood) was thus increased if the optimal transmit frequency was used.

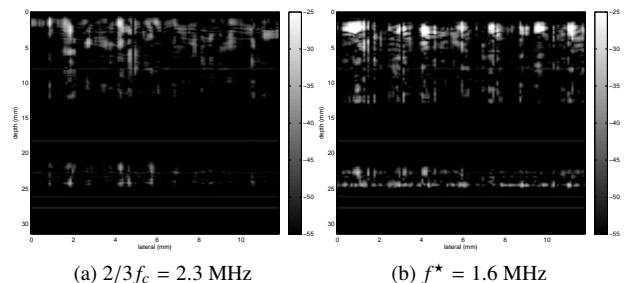


Figure 4: Synthetic Image where the transmit frequency was the two-thirds of the transducer centre frequency and the optimal frequency  $f^*$ .

## 4 Experimental Validation

The aim of this experiment was to confirm experimentally the results obtained in the simulation.

### 4.1 Experimental Setup

The experimental setup is presented in Fig. 1. The transmitted signal  $x_k(t)$  was first generated digitally using equation 2 by a personal computer. It was sent from an ultrasound scanner to the medium via an ultrasound probe. This wave insonified the medium. The reception system collected the echoes  $y_k(t)$  and filtered around  $2f_k$  to form a line of the harmonic image.

### 4.1.1 Ultrasound Scanner and Transducers

The transmitted signal  $x_k(t)$  was sent to an “open” ultrasound scanner (MultiX WM, M2M, Les Ulis, France) via USB. This ultrasound scanner automatically duplicated the signal  $x_k(t)$  for each element of the ultrasound probe. It applied the delays necessary to obtain phased-array beamforming [14]. The signals were then transmitted to a linear array of 128 elements (Vermon SA, Tours, France), centred at 4 MHz with a fractional bandwidth of 53% to  $-3$  dB. The wave focused on 28 mm from the surface. Note that the pulse was chosen with a cycle number corresponding to 55% of the relative bandwidth at the transducer centre frequency (*i.e.*  $N_c = 4$ ) and with a pressure level  $A_0$  of 400 kPa at the focal point.

### 4.1.2 Medium Explored

The wave propagated through a tissue-mimicking phantom (model 054GS, General Purpose Ultrasound Phantom, CIRS, Norfolk, VA, USA), including an hyperechoic target at a 4 cm-depth and with a 6 dB-contrast.

## 4.2 Experimental Results

The experimental results presented in Fig. 5 show the transmit frequency and the *CHFR* during the iterations. The error bars show the standard deviation of the *CHFR* in the image at the iteration  $k$ . The *CHFR* converged to its optimal value after six iterations for a transmit frequency of 2.1 MHz. The mean *CHFR* after convergence was around  $-32.8$  dB, *i.e.* a mean gain of 5.2 dB.

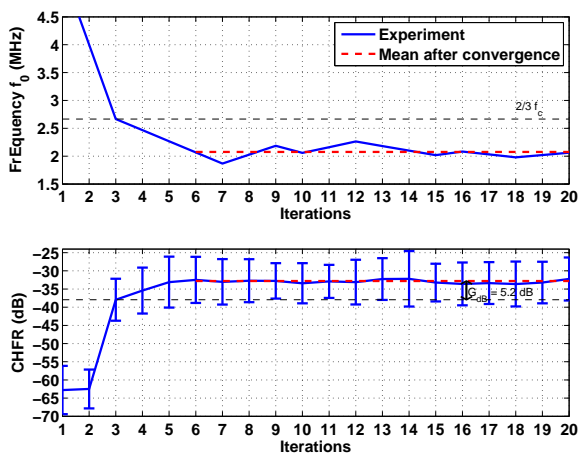


Figure 5: Automatic optimization experiment of *CHFR*

These results confirmed the experimental feasibility of the method. Note that there was a difference between the gain value in our simulation and that in our experiment. This difference may be explained by the different transducer properties. In simulation, the transducer centre frequency was lower than in experiment to decrease the simulation time.

As an illustration, the Fig. 6 represents the image for the two-thirds of the transducer centre frequency and the image for the optimal frequency  $f^*$  with logarithm compression. At the middle of the images, the hyperechoic target energy backscattered was increased to 12% with the optimal frequency. Moreover, the power ratio between the hyperechoic target and the surrounding medium was increased to

8%. The contrast was thus increased when the optimal transmit frequency was used.

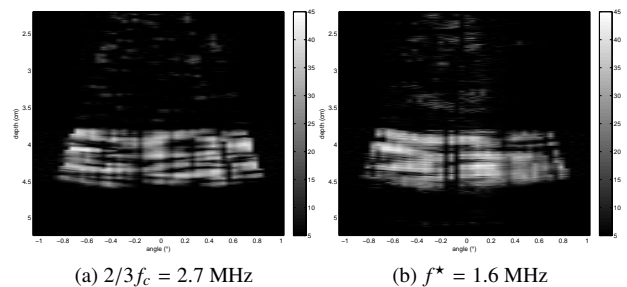


Figure 6: Experimental Image where the transmit frequency was the two-thirds of the transducer centre frequency and the optimal frequency  $f^*$ .

## 5 Discussions and Conclusion

*CHFR* optimization in tissue harmonic imaging was performed automatically, without taking into account *a priori* knowledge of the medium or the transducer, except for the first three values of the transmit frequency knowing that their selection had only impact on the convergence speed. The algorithm automatically determined an appropriate value for the transmit frequency within only a few iterations. To date, the recommended transmit frequency was the two-thirds of the transducer centre frequency, but this empirical setting cannot enable the optimum performances. The proposed algorithm itself adjusted the transmit frequency to maximize the harmonic power backscattered while minimizing the fundamental power backscattered within the transducer bandwidth.

Our method was easy to use for two reasons. Optimization was iteratively achieved by using first an easily implemented algorithm and by using second a single parameter. A major advantage of our approach is that it was independent of the medium explored since the cost-function was exclusively based on the input and the output measurements of our system. An interesting consequence is that our method can be applied to any imaging system.

Note that a real-time implementation was possible, since the computation time was insignificant. However, the method required a programmable analogue transmitter. Moreover, although our technique could offer an optimal frequency for each line of the image, it was preferable to perform optimization on the whole image. The image can be consistent with a single resolution.

To conclude, the method described ensured optimal *CHFR* by adaptively selecting the transmit frequency. Through our new approach, manufacturers and clinicians do not need to set themselves the transmit frequency.

Our closed-loop method can be adapted using a larger number of techniques for tissue harmonic imaging. The only difficulty remaining is in the instrumentation. However the development of new imaging methods based on chirp or time reversal are also needed for such instrumentation.

## References

- [1] P. J. A. Frinking, A. Bouakaz, J. Kirkhorn, F. J. Ten Cate, and N. de Jong. Ultrasound contrast imaging, Current and new potential methods. *Ultrasound Med. Biol.* **26**(6), 965–975 (2000).
- [2] F. Tranquart, N. Grenier, V. Eder, and L. Pourcelot. Clinical Use of Ultrasound Tissue Harmonic Imaging. *Ultrasound Med. Biol.*, 25(6), 889–894 (1999).
- [3] M. A. Averkiou. Tissue Harmonic Imaging. In *Proc. IEEE Ultrason. Symp.* **2**, 1563–1572 (2000).
- [4] Qingyu Ma, Xiufen Gong, and Dong Zhang. Third Order Harmonic Imaging for Biological Tissues using Three Phase-Coded Pulses. *Ultrasonics* **44**(Supplement), e61–e65 (2006).
- [5] D. H. Simpson, C. T. Chin, and P. N. Burns. Pulse Inversion Doppler: A New Method for Detecting Nonlinear Echoes from Microbubble Contrast Agents. *IEEE Trans. Ultrason., Ferroelectr., Freq. Control* **46**(2), 372–382 (1999).
- [6] Q. Ma, Y. Ma, X. Gong, and Dong Zhang. Improvement of Tissue Harmonic Imaging using the Pulse-Inversion Technique. *Ultrasound Med. Biol.* **31**(7), 889–894 (2005).
- [7] G. A. Brock-fisher, M. D. Poland, and P. G. Rafter. Means for Increasing Sensitivity in Non-linear Ultrasound Imaging Systems, *US Patent 5577505* (1996).
- [8] J. Song, S. Kim, H. Sohn, T. Song, and Yang Mo Yoo. Coded Excitation for Ultrasound Tissue Harmonic Imaging. *Ultrasonics* **50**(6), 613–619 (2010).
- [9] J. Song, J. H. Chang, T. Song, and Y. Yoo. Coded Tissue Harmonic Imaging with Nonlinear Chirp Signals. *Ultrasonics* **51**(4), 516–521 (2011).
- [10] J. A. Hossack, P. Mauchamp, and L. Ratsimandresy. A High Bandwidth Transducer Optimized for Harmonic Imaging. In *Proc. IEEE Ultrason. Symp.* **2**, 1021–1024 (2000).
- [11] S. Ménigot, A. Novell, I. Voicu, A. Bouakaz, and J.-M. Girault. Adaptive contrast imaging: Transmit frequency optimization. *Physics Procedia* **3**(1), 667–676 (2010).
- [12] S. Ménigot. *Commande optimale appliquée aux systèmes d'imagerie ultrasonore*. PhD thesis, Université François-Rabelais de Tours, Tours, France (2011).
- [13] B. Widrow and S. Stearns. *Adaptive Signal Processing*. Prentice Hall, Englewood Cliffs, USA (1985).
- [14] Thomas Szabo. *Diagnostic Ultrasound Imaging: Inside Out*. Academic Press, London, UK (2004).
- [15] M. E. Anderson. A 2D Nonlinear Wave Propagation Solver Written in Open-Source MATLAB Code. In *Proc. IEEE Ultrason. Symp.*, 1351–1354 (2000).